Efficient computation of natural convection in a concentric annulus between an outer square cylinder and an inner circular cylinder

C. Shu[1,*] and Y. D. Zhu[2]

[1]*Department of Mechanical and Production Engineering, National University of Singapore, 10 Kent Ridge Crescent, Singapore 119260*
[2]*Institute of High Performance Computing, 89C Science Park Drive #02-11/12, Singapore 118261*

SUMMARY

In this work, the natural convection in a concentric annulus between a cold outer square cylinder and a heated inner circular cylinder is simulated using the differential quadrature (DQ) method. The vorticity-stream function formulation is used as the governing equation, and the coordinate transformation technique is introduced in the DQ computation. It is shown in this paper that the outer square boundary can be approximated by a super elliptic function. As a result, the coordinate transformation from the physical domain to the computational domain is set up by an analytical expression, and all the geometrical parameters can be computed exactly. Numerical results for Rayleigh numbers range from 10^4 to 10^6 and aspect ratios between 1.67 and 5.0 are presented, which are in a good agreement with available data in the literature. It is found that both the aspect ratio and the Rayleigh number are critical to the patterns of flow and thermal fields. The present study suggests that a critical aspect ratio may exist at high Rayleigh number to distinguish the flow and thermal patterns. Copyright © 2002 John Wiley & Sons, Ltd.

KEY WORDS: differential quadrature method; natural convection; concentric annulus

INTRODUCTION

Natural convective heat transfer in horizontal annuli has attracted many attentions in recent years due to its wide applications such as in nuclear reactor design, cooling of electronic equipment, aircraft cabin insulation and thermal storage system. A large and diverse number of literatures on both experimental and numerical investigations were published in the past few decades. Among them, the majority was involved in horizontal circular annuli. Natural convective heat transfer in horizontal annuli between two concentric circular cylinders has been well studied. A comprehensive review was presented by Kuehn and Goldstein [1].

Comparatively, little work has been done on natural convective heat transfer in more complex annuli such as the problem considered in this study. A few publications were involved in

---

the experimental study. Warrington and Powe [2] reported some experimental results of natural convective heat transfer between concentrically mounted bodies (spheres, cylinders and cubes) at low Rayleigh numbers. Ekundayo *et al.* [3] studied natural convection in horizontal annulus between an outer square cylinder and an inner circular cylinder. In their study, a cylindrical heater with diameter of 9.5 mm was placed at different locations within a 350 mm × 350 mm square-sectioned cold enclosure. The aspect ratio, i.e., the side length of the outer square cylinder over the diameter of the inner cylinder, is 36.84, which is large. It was found that the maximum steady-state rate of natural convection occurred when the heater was located parallel to and near a vertical wall.

A few publications were also found for numerical investigations. Stella and Guj [4] studied fluid flow and heat transfer in a multi-connected driven cavity using a finite difference method. Ghaddar [5], Deschamps and Desrayaud [6] studied natural convective heat transfer from a uniformly heated horizontal cylinder placed in a large air-filled rectangular enclosure. The aspect ratio in their studies is also large. Moukalled and Acharya [7] studied numerically natural convective heat transfer from a heated horizontal cylinder placed concentrically inside a square enclosure. The governing equations in their work are solved in a body-fitted coordinate system using a control volume-based numerical procedure. Liu *et al.* [8] studied the coupled heat conduction/convection problem for a solid cylinder in either a rectangular or a circular enclosure filled with air using an operator-splitting pseudo-time-stepping finite element method.

In the previous studies for numerical simulation of natural convection in a complex annulus, low order methods such as finite difference, finite volume and finite element methods are usually used. In general, the low order methods need to use a large number of grid points to obtain accurate numerical results, and, as a consequence, require large computational effort possibly and virtual storage. In the present study, the natural convection in a concentric annulus between an outer square cylinder and a heated inner circular cylinder is numerically studied using the differential quadrature (DQ) method. DQ is a global method for numerical discretization, which can be applied to discretize the derivatives in both the governing equations and the boundary conditions. The feature of the DQ method is that it can obtain very accurate numerical results by using a considerably small number of grid points and requiring very little computational effort. Like the conventional low order finite difference schemes, the DQ method also requires the computational domain to be regular. It has been shown by many researchers (Bellman *et al.* [9], Shu *et al.* [10–15], Bert and Malik [16]) that the application of the DQ method to regular domain problems is very efficient. Now, the DQ method is well accepted in the computational mechanics, especially in the solid mechanics. On the other hand, we note that there are very few works so far involving the application of the DQ method to irregular domain problems. The reason is that the DQ method cannot be directly applied to such cases. For irregular domain problems such as the one considered in this study, the coordinate transformation technique should be introduced. In this technique, the irregular physical domain is first transformed into a regular computational domain, and the governing equations as well as the boundary conditions are transformed into the relevant forms in the computational space. Then all the computations including the discretization of derivatives by the DQ method are based on the computational space. In this paper, we will show that the application of the DQ method to irregular domain problems is also very efficient. It is indicated that another important contribution of the present work is the introduction of a super elliptic function for the outer square boundary. With the super elliptic function, the coordinate transformation from the physical space to the computational space can be set up

by an analytical expression. Thus, all the geometrical parameters can be computed exactly. In the present study, the vorticity-stream function formulation is employed as the governing equation, and the SOR iteration method is applied to solve the resultant algebraic equations.

DIFFERENTIAL QUADRATURE METHOD

The DQ method is a global numerical approach proposed by Bellman *et al.* [9, 17], and greatly improved by Shu and Richards [10, 11] and Shu and Chew [14] in the development of explicit formulations for computing the weighting coefficients. For brevity, a one-dimensional problem is chosen in the following to demonstrate the DQ method, where the first- and second-order derivatives of $f(x)$ at a point x_i are approximated by

$$f_x(x_i) = \sum_{j=1}^{N} a_{ij} \cdot f(x_j), \quad \text{for } i = 1, 2, \ldots, N \tag{1}$$

$$f_{xx}(x_i) = \sum_{j=1}^{N} b_{ij} \cdot f(x_j), \quad \text{for } i = 1, 2, \ldots, N \tag{2}$$

Here N is the number of grid points, a_{ij} and b_{ij} are respectively the first- and second-order weighting coefficients. It is noted that Equations (1) and (2) are similar except that they use different weighting coefficients. Obviously, the key procedure in the DQ method is to determine the weighting coefficients a_{ij} and b_{ij}. It was shown by Shu and Richards [10, 11] and Shu and Chew [14] that all the ways of computing the weighting coefficients can be generalized under the analyses of function approximation and linear vector space. It was found that when the function $f(x)$ is approximated differently, the formulations for a_{ij} and b_{ij} are also different. In the following, the respective formulations of a_{ij} and b_{ij} are presented when the function $f(x)$ is approximated by a high order polynomial or by the Fourier series expansion.

Polynomial-Based Differential Quadrature (PDQ)

In this case, it is supposed that the function is approximated by a $(N-1)$th degree polynomial in the form

$$f(x) = \sum_{k=0}^{N-1} c_k \cdot x^k \tag{3}$$

Under the analysis of a linear vector space, Shu and Richards [10, 11] derived the following explicit formulations for computing the weighting coefficients

$$a_{ij} = \frac{M^{(1)}(x_i)}{(x_i - x_j) \cdot M^{(1)}(x_j)}, \quad \text{when } j \neq i \tag{4a}$$

$$a_{ii} = - \sum_{k=1, k \neq i}^{N} a_{ik} \tag{4b}$$

$$b_{ij} = 2a_{ij} \cdot \left(a_{ii} - \frac{1}{x_i - x_j} \right), \quad \text{when } j \neq i \tag{5a}$$

$$b_{ii} = - \sum_{k=1, k \neq i}^{N} b_{ik} \tag{5b}$$

where

$$M^{(1)}(x_i) = \prod_{k=1, k \neq i}^{N} (x_i - x_k)$$

It is indicated that a recurrence relationship has also been derived to compute the weighting coefficients of the higher order derivatives. For details, see the book of Shu [18].

Fourier Expansion-Based Differential Quadrature (FDQ)

In this case, the function is approximated by a Fourier series expansion in the form

$$f(x) = c_0 + \sum_{k=1}^{N/2} (c_k \cos kx + d_k \sin kx) \tag{6}$$

Similar to PDQ, Shu and Chew [14] and Shu and Xue [15] also derived the explicit formulations to compute the weighting coefficients a_{ij} and b_{ij}, which are listed below

$$a_{ij} = \frac{1}{2} \cdot \frac{P(x_i)}{\sin \frac{x_i - x_j}{2} \cdot P(x_j)}, \quad \text{when } j \neq i \tag{7a}$$

$$a_{ii} = - \sum_{k=1, k \neq i}^{N} a_{ik} \tag{7b}$$

$$b_{ij} = a_{ij} \left[2a_{ii} - ctg \frac{x_i - x_j}{2} \right], \quad \text{when } j \neq i \tag{8a}$$

$$b_{ii} = - \sum_{k=1, k \neq i}^{N} b_{ik} \tag{8b}$$

where

$$P(x_i) = \prod_{k=0, k \neq i}^{N} \sin \frac{x_i - x_k}{2}$$

It should be indicated that Equations (7) and (8) can be applied to the periodic problems and the non-periodic problems. For the non-periodic problems, the x range in the computational domain is $0 \leqslant x \leqslant \pi$, while for the periodic problems, the x range in the computational domain is $0 \leqslant x < 2\pi$. For details, refer to the book of Shu [18].

It should be indicated that unlike low order methods, it is very difficult to do stability analysis for PDQ and FDQ methods. In the present study, the PDQ and FDQ methods will be used to discretize the spatial derivatives in the governing equations and the boundary conditions. The derivatives in the radial direction are discretized by the PDQ method while the derivatives in the circumferential direction are discretized by the FDQ method.

GOVERNING EQUATIONS AND BOUNDARY CONDITIONS

A schematic view of a horizontal concentric annulus between an outer square cylinder and a heated inner circular cylinder is shown in Figure 1. Heat is generated uniformly within the inner circular cylinder, the outer square cylinder is concentrated with the inner cylinder and is cold. The imposed boundary conditions are no-slip and isothermal on both cylinder walls. As the cylinders are long enough, the flow is considered to be steady, laminar and two-dimensional. The buoyancy force is the driven force for the flow. Based on the Boussinesq approximation, the non-dimensional governing equation for the problem is written in the vorticity-stream function formulation [19] as

$$\frac{\partial^2 \psi}{\partial x^2} + \frac{\partial^2 \psi}{\partial y^2} = \omega \tag{9}$$

$$u\frac{\partial \omega}{\partial x} + v\frac{\partial \omega}{\partial y} = Pr\left(\frac{\partial^2 \omega}{\partial x^2} + \frac{\partial^2 \omega}{\partial y^2}\right) - Pr\,Ra\frac{\partial T}{\partial x} \tag{10}$$

$$u\frac{\partial T}{\partial x} + v\frac{\partial T}{\partial y} = \frac{\partial^2 T}{\partial x^2} + \frac{\partial^2 T}{\partial y^2} \tag{11}$$

where ψ denotes stream function, ω represents vorticity, T is non-dimensional temperature. Prandtl number is defined as $Pr = \mu C_P/k$, Rayleigh number is defined as $Ra = C_p\rho_0 g\beta L^3 \Delta T^*/(kv)$. Here μ is viscosity, C_p is specific heat at constant pressure, k is thermal diffusivity, ρ_0 is reference density, g is gravity acceleration, β is thermal expansion coefficient, L is the side length of the outer square cylinder, ΔT^* is the temperature difference between inner and outer cylinders, v is kinematic viscosity.
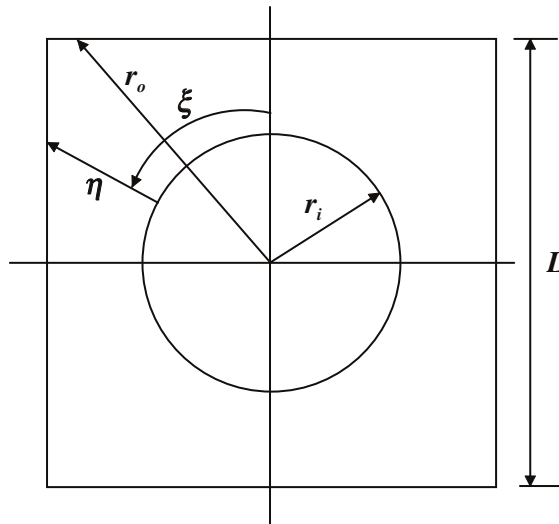

Figure 1. Sketch of physical domain.

The non-dimensionalization is taken in the following way:

$$T = \frac{T^* - T_o^*}{\Delta T^*}, \quad \omega = \frac{\omega^* L^*}{v_\infty^*}, \quad \psi = \frac{\psi^*}{L^* v_\infty^*}, \quad v_\infty^* = \frac{k}{L}$$

where T^*, T_o^*, ω^*, v_∞^*, L^* and ψ^* are the dimensional temperature, outer boundary temperature, vorticity, reference velocity, reference length and stream function respectively. The dimensional temperature difference is $\Delta T^* = T_i^* - T_o^*$, where T_i^* is dimensional temperature at the inner boundary. Velocity components u and v can be computed from the stream function ψ as

$$u = \frac{\partial \psi}{\partial y}, \quad v = -\frac{\partial \psi}{\partial x} \tag{12}$$

Using the expressions in Equation (12), Equation (9) can be written as

$$\omega = \frac{\partial u}{\partial y} - \frac{\partial v}{\partial x} \tag{13}$$

Like the low order finite difference schemes, the DQ method requires the physical boundary to be a mesh line. In the present study, however, the physical boundaries may not coincide with the mesh lines. When the DQ method is applied to this case, the physical boundary conditions cannot be implemented in a straightforward way. To overcome this difficulty, the following transformation from the physical space to the computational space is required

$$\begin{cases} \xi = \xi(x, y) \\ \eta = \eta(x, y) \end{cases} \tag{14}$$

With this transformation, the governing Equations (9)–(11) can be transformed to the following forms in the computational space

$$A\frac{\partial^2 \psi}{\partial \xi^2} + 2B\frac{\partial^2 \psi}{\partial \eta \, \partial \xi} + C\frac{\partial^2 \psi}{\partial \eta^2} + G\frac{\partial \psi}{\partial \eta} + H\frac{\partial \psi}{\partial \xi} = J\omega \tag{15}$$

$$U\frac{\partial \omega}{\partial \xi} + V\frac{\partial \omega}{\partial \eta} = Pr\left(A\frac{\partial^2 \omega}{\partial \xi^2} + 2B\frac{\partial^2 \omega}{\partial \xi \, \partial \eta} + C\frac{\partial^2 \omega}{\partial \eta^2} + G\frac{\partial \omega}{\partial \eta} + H\frac{\partial \omega}{\partial \xi}\right)$$
$$- Pr\, Ra\left(y_\eta \frac{\partial T}{\partial \xi} - y_\xi \frac{\partial T}{\partial \eta}\right) \tag{16}$$

$$U\frac{\partial T}{\partial \xi} + V\frac{\partial T}{\partial \eta} = \left(A\frac{\partial^2 T}{\partial \xi^2} + 2B\frac{\partial^2 T}{\partial \xi \, \partial \eta} + C\frac{\partial^2 T}{\partial \eta^2} + G\frac{\partial T}{\partial \eta} + H\frac{\partial T}{\partial \xi}\right) \tag{17}$$

where

$$U = \frac{\partial \psi}{\partial \eta} = u y_\eta - v x_\eta, \qquad V = -\frac{\partial \psi}{\partial \xi} = v x_\xi - u y_\xi$$

$$A = \alpha/J, \qquad\qquad B = -\sigma/J$$

$$C = \gamma/J, \qquad\qquad G = \frac{\partial B}{\partial \xi} + \frac{\partial C}{\partial \eta}$$

$$H = \frac{\partial A}{\partial \xi} + \frac{\partial B}{\partial \eta}, \qquad \alpha = x_\eta^2 + y_\eta^2$$

$$\sigma = x_\xi x_\eta + y_\xi y_\eta, \qquad \gamma = x_\xi^2 + y_\xi^2$$

$$J = x_\xi y_\eta - y_\xi x_\eta$$

From the no-slip condition, the velocities U and V on both the inner and outer cylinder walls are zero. For a concentric annulus, the stream function values on the inner and outer cylinders are the same due to the symmetry of flow field. The stream function value on both cylinder walls is set to zero in the present study. The boundary conditions can be written as

$$U|_{\eta=0,1} = 0, \qquad V|_{\eta=0,1} = 0 \qquad\qquad (18a)$$

$$\psi|_{\eta=0} = 0, \qquad \psi|_{\eta=1} = 0 \qquad\qquad (18b)$$

$$T|_{\eta=0} = 1, \qquad T|_{\eta=1} = 0 \qquad\qquad (18c)$$

The boundary condition for vorticity ω can be derived from Equation (15) and written as

$$\omega\bigg|_{\eta=0,1} = \frac{C}{J} \frac{\partial^2 \psi}{\partial \eta^2}\bigg|_{\eta=0,1} = \frac{C}{J} \frac{\partial U}{\partial \eta}\bigg|_{\eta=0,1} \qquad\qquad (19)$$

The Neumann boundary condition for the stream function can be derived from Equation (18a) and written as

$$\frac{\partial \psi}{\partial \eta}\bigg|_{\eta=0,1} = 0 \qquad\qquad (20)$$

In the ξ direction, the periodic condition is used, which is automatically implemented by the FDQ method.

SUPER ELLIPTIC FUNCTION AND ANALYTICAL COORDINATE TRANSFORMATION

As shown in Figure 1, the physical domain is formed by a square outer cylinder and a circular inner cylinder. The DQ method cannot be directly applied to solve this problem in both the

Cartesian coordinate system and the cylindrical coordinate system. To apply the DQ method, we have to do the coordinate transformation, which maps the physical domain to a rectangular domain in the computational space. Usually, the coordinate transformation is made by using the numerical grid generation technique. In this technique, the geometrical parameters such as x_ξ, x_η, y_ξ and y_η are approximated by a numerical discretization technique. Obviously, this treatment will introduce additional numerical errors into the computation, which may have some effects on the accuracy of numerical results. As will be shown below, the super elliptic function can be used to accurately approximate a rectangular boundary. So, for the problem considered in this study, an analytical expression can be derived for the coordinate transformation from the physical space to the computational space. Then all the geometrical parameters can be computed exactly. The super elliptic function can be written as

$$\left(\frac{x}{a}\right)^{2n} + \left(\frac{y}{b}\right)^{2n} = 1 \tag{21}$$

where a and b are half of the elliptic lengths in x and y direction respectively, n is a positive integer. It is interesting to see that when $n=1$, $a \neq b$, the geometry represented by Equation (21) is an ellipse; and when $n=1$, $a=b$, the geometry becomes a circle. As n increases from 1, the geometry would approach a rectangle when $a \neq b$ or a square when $a=b$. The geometries varying with n for $a=b$ are shown in Figure 2. It can be concluded that when n is above 20, the geometry keeps very little change with the increase of n and remains in a square with tiny round corner. Therefore the non-dimensional square outer cylinder can be approximated by

$$x^{2n} + y^{2n} = 1 \tag{22}$$

with the use of a large value of n.

   The relationship between the geometric error l of a square approximated by the super elliptic function and n is shown in Figure 3. The error l is defined in this way. Let s stand for half of the diagonal length of the square, which is calculated as $s = \sqrt{2}$, r represent half of the diagonal length approximated by the super elliptic function which can be expressed as
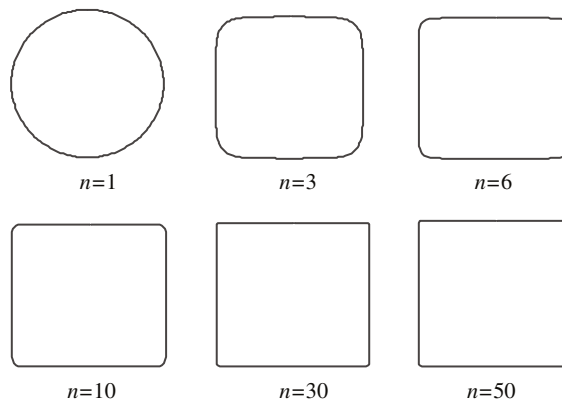

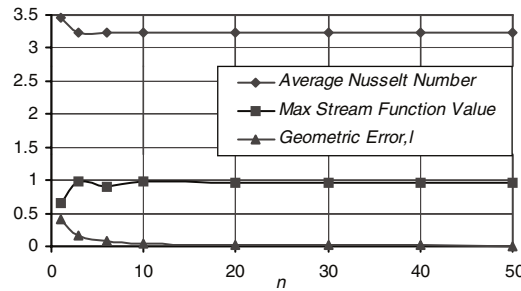Figure 2. Effect of power n on geometry.

Figure 3. Effect of power n on geometric approximation and $Nu, \psi_{\max}$ for $Ra = 10^4$, $rr = 2.5$.

$r = 2^{[(1/2)-(1/2n)]}$ from Equation (22). The error l is then defined as

$$l = 2^{1/2} \cdot (1 - 2^{-1/2n}) \tag{23}$$

It can be seen from Figure 3 that as n increases, the error decreases. When n increases from 1 to 5, the error drops very fast. After that, the reduction of the error is very slow.

By defining the accuracy on geometry as $\varepsilon = (l/s)$, Equation (23) can be rewritten as

$$n \geqslant -\frac{\ln 2}{2 \cdot \ln(1 - \varepsilon)} \tag{24}$$

If ε is set as 0.01, then n must be larger than 35. In the present study, the power n is set as 50.

With Equation (22), the coordinate transformation for the present problem can be exactly set up, which is written as

$$x = -\sin \xi \cdot [r_i + (r_o - r_i)\eta] \tag{25a}$$

$$y = \cos \xi \cdot [r_i + (r_o - r_i)\eta] \tag{25b}$$

where r_i is the radius of the inner cylinder, which is a constant, r_o is computed from Equation (22) as

$$r_o = \frac{1}{(\cos^{2n} \xi + \sin^{2n} \xi)^{1/2n}} \tag{26}$$

The transformed computational domain in the (ξ, η) plane is $0 \leqslant \eta \leqslant 1$ and $0 \leqslant \xi \leqslant 2\pi$.

DEFINITION OF NUSSELT NUMBER

The local heat transfer rate on the inner cylinder can be computed by

$$q = h(T_i^* - T_o^*) = -k \frac{\partial T^*}{\partial n} \tag{27}$$

where h represents the local heat transfer coefficient, k is the thermal diffusivity. From Equation (27), we can get

$$h = -k\frac{\partial T}{\partial n} \tag{28}$$

Since

$$\frac{\partial T}{\partial n} = \frac{\gamma(\partial T/\partial \eta) - \beta(\partial T/\partial \xi)}{J\sqrt{\gamma}} = \frac{\partial T}{\partial \eta} \cdot \frac{\sqrt{\gamma}}{J} \tag{29}$$

where $(\partial T)/(\partial \xi) = 0$ is applied at the boundary, Equation (28) can be simplified to

$$h = -k\frac{\partial T}{\partial \eta} \cdot \frac{\sqrt{\gamma}}{J} \tag{30}$$

With Equation (30), the average heat transfer coefficient $\bar{h}$ can be computed as

$$\bar{h} = \frac{1}{2\pi}\int_0^{2\pi} h \cdot \mathrm{d}\xi \tag{31}$$

And the average Nusselt numbers for the outer and inner boundaries are respectively determined by

$$\begin{cases} \bar{N}u_i = \dfrac{\bar{h}_i S_i}{k} \\ \bar{N}u_o = \dfrac{\bar{h}_o S_o}{k} \end{cases} \tag{32}$$

where S_i and S_o are defined in the same way as in the work of Moukalled and Acharya [7]. In their work, the computational domain is taken as half of the physical domain due to the symmetry, so S_i and S_o are taken as half of the circumferential lengths of the inner and outer cylinder surfaces respectively. Since at steady state, the Nusselt numbers along the inner and outer walls are the same, there is no need to pay separate attention to $\bar{N}u_i$ and $\bar{N}u_o$. Thus in this study, we only show the value of $\bar{N}u_i$, which is also noted as $\bar{N}u$.

RESULTS AND DISCUSSION

In the present study, air is considered to be the working fluid and the Prandtl number is fixed at 0.71. The cases for three different aspect ratios ($rr = L/2r_i = 5.0, 2.5, 1.67$) and Rayleigh numbers of 10^4, 5×10^4, 10^5, 5×10^5 and 10^6 were studied. The power n used in the super elliptic function is taken to be 50 for a good approximation of the square boundary. The PDQ method is applied in the η direction with non-uniform grid point distribution, while the FDQ method is applied in the ξ direction with uniform grid point distribution. The grid point distributions are taken as

$$\xi_i = \frac{i-1}{N} \cdot 2\pi, \quad i = 1, 2, \ldots, N \tag{33a}$$

$$\eta_j = \frac{1}{2}\left[1 - \cos\left(\frac{j-1}{M-1}\pi\right)\right], \quad j = 1, 2, \ldots, M \tag{33b}$$

After numerical discretization by the DQ method, the resultant algebraic equations are solved by the SOR iteration method. The convergence criteria are chosen as $|R_\psi|_{\max} \leqslant 10^{-4}, |R_T|_{\max} \leqslant 10^{-4}$ and $|R_\omega|_{\max} \leqslant 10^{-2}$ for ψ, T and ω equations respectively, where $|R_\psi|_{\max}$, $|R_T|_{\max}$ and $|R_\omega|_{\max}$ are the maximum absolute residual values for the stream function, temperature and vorticity equations respectively. When all the three criteria are satisfied, the convergent results are subsequently obtained. The convergence criteria are found to be sufficiently stringent and the numerical results are changed by less than 0.01 per cent when stricter criteria are used. In the present study, the initial values are set to zero for all ψ, u, v, T and ω at interior points.

Grid-independent study

The grid-independence of numerical results is studied for the case of $Ra = 10^5$, $rr = 2.5$, $Pr = 0.71$. The six mesh sizes of 21×11, 25×15, 31×17, 31×19, 33×19, 31×21 are used to do grid-independence study. It is noted that the total number of grid points for the above six mesh sizes is respectively 231, 375, 527, 589, 627 and 651. Numerical experiments showed that when the mesh size is above 31×19 (589 points), the computed $\psi_{\max}$ and $\bar{N}u$ remain the same. This can be seen clearly in Figure 4, which shows $\bar{N}u$ and $\psi_{\max}$ versus the total number of grid points. When the number of mesh points is above 589, $\bar{N}u$ remains at 4.86 and $\psi_{\max}$ is kept at 8.10. Apart from the high accuracy of numerical results, the numerical computation is also very fast. For all the six mesh sizes, the CPU time required on SGI 2400 is less than 1 s. In fact, the actual run time for the six cases is within a few minutes. The run time for mesh sizes of 21×11, 25×15, 31×17, 31×19, 33×19, 31×21 is respectively $37.5, 99.3, 191.9, 305.1, 359.8$ and 373.1 s. Since the number of unknowns is very small, and the resultant algebraic equations are solved by SOR iteration method which does not need to store the matrix of the equation system, the memory requirement of present computation is very little.

On the other hand, we should indicate that the minimum mesh size for a grid-independent solution depends on the complexity of the flow, temperature fields and the aspect ratio. In order to save the computational effort and obtain accurate numerical results, one has to balance the use of mesh size for the given Ra and rr. From our numerical experiments, it was found that for the moderate Ra, 31×21 grid points are adequate to yield very accurate results. When Ra increases, more grid points should be used to obtain accurate results. In this study, the mesh sizes of 31×21, 41×21 and 69×39 are used respectively for $Ra = 10^4, 10^5, 10^6$.
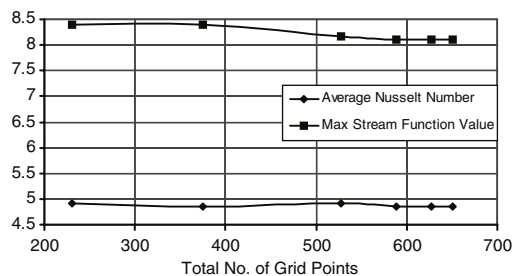

Figure 4. $Nu, \psi_{\max}$ versus total number of grid points for $Ra = 10^5$, $rr = 2.5$.

Effect of power n on numerical results

The effect of power n of the super elliptic function on the approximation of geometry has been studied in the previous section, and some results are displayed in Figure 3. It was shown that the accuracy of geometry approximation can reach to 0.01 when the power n is taken to be 35. In this section, we will study the effect of power n on the numerical results. Figure 3 also displays the change of $\bar{N}u$ and ψ_{max} with increase of the power n for the case of $Ra = 10^4$ at aspect ratio $rr = 2.5$. It is clearly shown in the figure that $\bar{N}u$ and ψ_{max} remain the same when the power n of the super elliptic function exceeds 10 and 20 respectively. This shows that accuracy of the numerical results is less sensitive to the power n than the accuracy of geometry approximation. For accurate numerical results and good geometry approximation, the power n is taken to be 50 in the following study.

Validation of numerical results

As discussed in the introduction, most research work focused on the study of natural convection in annuli between either concentric or eccentric circular cylinders. Only a few publications involve the study of natural convection in an annulus between an outer square cylinder and an inner circular cylinder. The work of Moukalled and Acharya [7] is one of such studies. Moukalled and Acharya [7] studied numerically natural heat transfer between a heated horizontal cylinder placed concentrically inside a square enclosure. Three different aspect ratios and four different Rayleigh numbers were considered. The governing equations were solved in a body-fitted coordinate system using a control volume-based numerical procedure. Their numerical data were validated by comparison with some experimental data and found in a good agreement. Thus, in this study, the results of Moukalled and Acharya [7] are used to validate the present numerical results. The maximum stream function value ψ_{max} and the average Nusselt number $\bar{N}u$ between the present work and the work of Moukalled and Acharya [7] are compared in Table I for Rayleigh numbers of $10^4, 10^5, 10^6$ and aspect ratios of 5.0, 2.5 and 1.67. It should be noted that due to the different ways of non-dimensionalization between Moukalled and Acharya [7] and the author, the equivalent ψ_{max} in Table I is the one from

Table I. Comparison of ψ_{max} and $\bar{N}u$.

Item	rr	Ra	ψ_{max}		$\bar{N}u$	
			Present	Moukalled and Acharya [7] (Equivalent)	Present	Moukalled and Acharya [7]
1	5.0		1.71	1.73	2.08	2.071
2	2.5	10^4	0.97	1.02	3.24	3.331
3	1.67		0.49	0.50	5.40	5.826
4	5.0		9.93	10.15	3.79	3.825
5	2.5	10^5	8.10	8.38	4.86	5.08
6	1.67		5.10	5.10	6.21	6.212
7	5.0		20.98	25.35	6.11	6.107
8	2.5	10^6	24.13	24.07	8.90	9.374
9	1.67		20.46	21.30	12.00	11.62

Moukalled and Acharya [7] multiplied by the Prandtl number. It is noted that the reference length used in the Rayleigh number is the side length of square, L. From Table I, it can be seen that the present results generally agree well with those of Moukalled and Acharya [7]. From the grid-independent study of the present work, it is believed that the present numerical results are more accurate than those of Moukalled and Acharya [7].

Analysis of flow and thermal fields

The DQ method has been demonstrated in the above sections to be very efficient which can obtain accurate results using very few mesh points. With the confidence of the DQ method, the flow and thermal fields for 15 cases of $Ra = 10^4, 5 \times 10^4, 10^5, 5 \times 10^5, 10^6$ and $rr = 5.0, 2.5, 1.67$ are numerically analysed. The values of $\psi_{max}, \bar{Nu}$ and maximum velocity $\bar{U}_{max}$ for these 15 cases are listed in Table II. The average Nusselt number versus Rayleigh number at different aspect ratios is shown in Figure 5. The respective streamlines and isotherms are shown in Figure 6. A typical velocity vector for the case of $Ra = 10^5$, $rr = 2.5$ is shown in Figure 7. It is found that both the aspect ratio and the Rayleigh number are critical to the flow and thermal fields.

For the streamlines shown in Figure 6(a), it can be observed that the flow is generally symmetrical about the vertical centre line through the centre of the inner circular cylinder. It moves up along the inner heated circular cylinder. When the flow reaches the top of the outer square cylinder, it then moves horizontally outwards and goes down along the vertical

Table II. Computational Results of $\bar{Nu}$, ψ_{max} and $\bar{U}_{max}$.

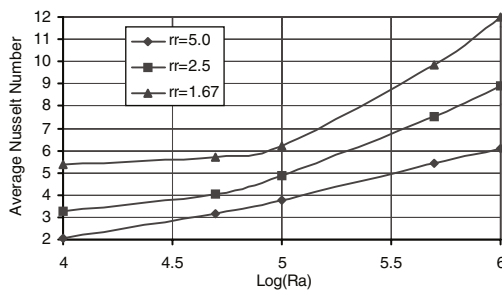| Item	Ra	Aspect Ratio rr								
		5.0			2.5			1.67		
		$\bar{Nu}$	ψ_{max}	$\bar{U}_{max}$	$\bar{Nu}$	ψ_{max}	$\bar{U}_{max}$	$\bar{Nu}$	ψ_{max}	$\bar{U}_{max}$
1	10^4	2.08	1.71	5.51	3.24	0.97	2.71	5.40	0.49	1.09
2	5×10^4	3.17	6.63	20.71	4.02	4.82	13.25	5.68	2.66	5.78
3	10^5	3.79	9.93	32.03	4.86	8.10	22.81	6.21	5.10	11.25
4	5×10^5	5.40	18.28	76.77	7.53	19.66	61.38	9.83	14.55	35.50
5	10^6	6.11	20.98	117.68	8.90	24.13	79.81	12.00	20.46	53.80

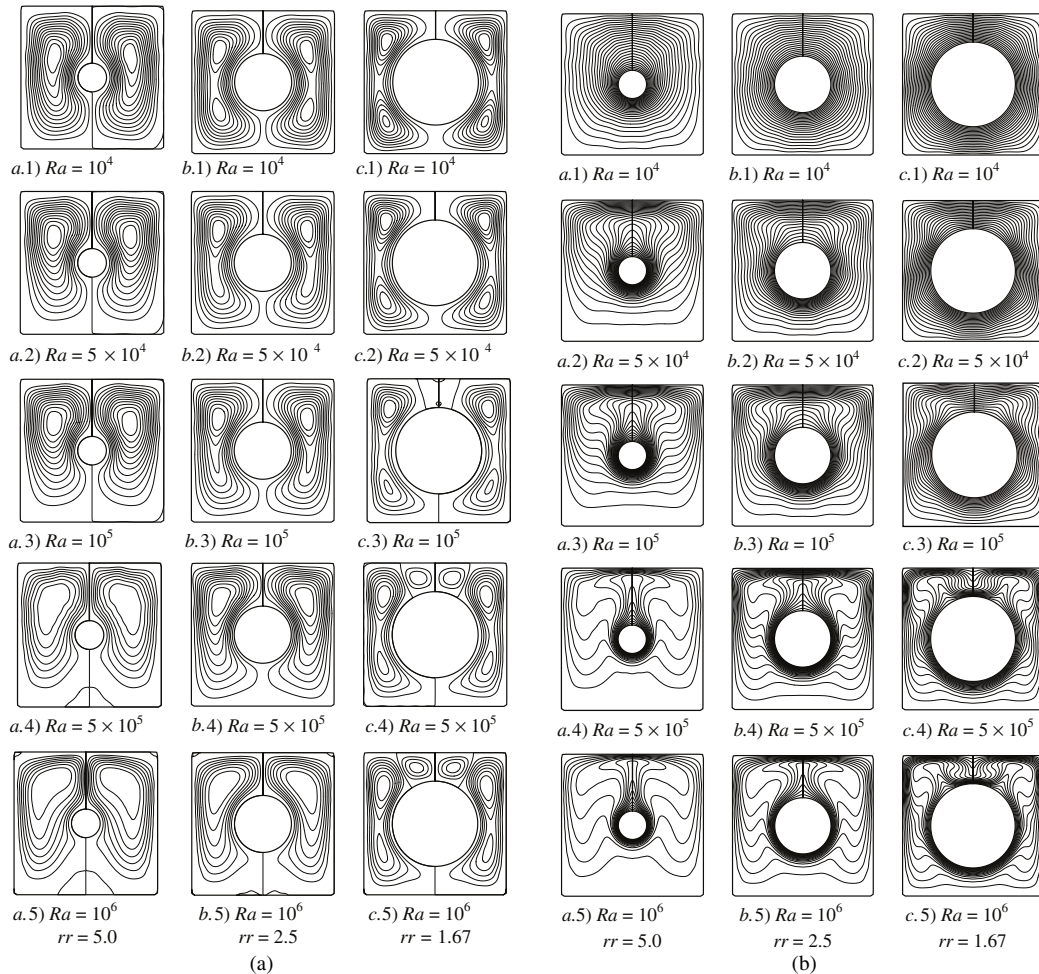Figure 5. Average Nusselt number versus Rayleigh number.

Figure 6. (a) Streamlines; (b) Isotherms.

sidewall of the outer square cylinder. For the isotherms as shown in Figure 6(b), it can be seen that the heat transfer is mainly dominated by conduction at low Rayleigh numbers, and by convection at high Rayleigh numbers. The details are discussed.

For the case of $rr = 5.0$, the inner circular cylinder is small as compared to the outer square cylinder and the physical domain between the inner and outer cylinders is large. At Rayleigh number of 10^4, the maximum stream function is very small, and the circulation of the flow is very weak. For this case, the heat transfer is mainly dominated by conduction and a little stagnant area exists near the bottom of the square cylinder. The flow velocity is too small to affect the temperature distribution. As the Rayleigh number increases, the circulation of the flow becomes stronger and stronger. As a result, the maximum stream function value is increased from 1.71 at $Ra = 10^4$ to 20.98 at $Ra = 10^6$. The centres of the two symmetric eddies move upward from about $70°$ at $Ra = 10^4$ to about $35°$ at $Ra = 10^6$. Clearly, the two eddies
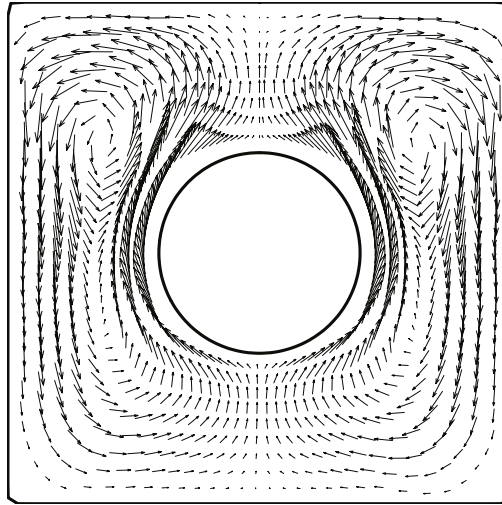
Figure 7. Velocity vector for the case of $Ra = 10^5$, $rr = 2.5$.

move closer and closer with the increase of Rayleigh number. When the Rayleigh number is increased from 10^4 to above 5×10^4, a plume begins to appear on top of the inner circular cylinder. As the Rayleigh number increases, the stagnant area increases at the bottom of the outer square cylinder, and the thermal boundary layer becomes thinner and thinner. So, the overall Nusselt number increases with the Rayleigh number.

For the case of $rr = 2.5$, the inner circular cylinder becomes bigger and the physical domain between the inner and outer cylinders is reduced. Generally, the patterns of streamlines and isotherms for this case are the same as those for the aspect ratio of $rr = 5.0$. At low Rayleigh numbers, the heat transfer is mainly dominated by the conduction. As the Rayleigh number increases, the convection part plays a more and more important role in the heat transfer. At high Rayleigh numbers, the heat transfer is mainly dominated by the convection. The behaviour of ψ_{max} and $\bar{N}u$ with the Rayleigh number for this case is the same as that for the case of $rr = 5.0$, That is, as the Rayleigh number increases, both ψ_{max} and $\bar{N}u$ increase. On the other hand, if we compare the values of ψ_{max} and $\bar{N}u$ for this case and the case of $rr = 5.0$ under the same Rayleigh number, we find that as the aspect ratio decreases, ψ_{max} is reduced while $\bar{N}u$ is increased. This indicates that when the aspect ratio is reduced, the circulation of the flow becomes weaker, but the heat transfer becomes stronger. The reason is probably due to the reduction in size of the computational domain. The small size of the domain may limit the heat flow and ease the heat transfer by conduction.

For the case of $rr = 1.67$, the inner circular cylinder is further enlarged and the physical domain between the inner and outer cylinders is further reduced. The patterns of streamlines and isotherms for this case are different from those for the cases of $rr = 5.0$ and $rr = 2.5$. At Rayleigh number of 10^4, the circulation of the flow is also very weak, and the maximum stream function value is small. As the Rayleigh number increases, the maximum stream function value and the average Nusselt number also increase, and four eddies are gradually formed, which are still symmetrical about the vertical centre line. The two tiny eddies

appear near the vertical centre line when the Rayleigh number reaches 10^5. Further, when the Rayleigh number is increased to above 10^5, two plumes instead of one begin to appear on top of the inner circular cylinder with about $40°$ from the vertical centre line. As Rayleigh number increases to above 5×10^5, the two plumes become bigger, and a third plume appears above top of the inner cylinder with reverse direction. The two tiny eddies on top of the inner cylinder probably cause the formation of the third plume to appear in the reverse direction.

From the above discussion, it is clear that the aspect ratio and Rayleigh number greatly affect the flow and thermal fields. As the Rayleigh number increases, the circulation of the flow is enhanced, and the thermal plume is formed. For $rr = 5.0$ and $rr = 2.5$, only one plume is formed on top of the inner cylinder and two eddies exist symmetrically about the vertical centre line. However, for $rr = 1.67$, two plumes and one additional plume in the opposite direction are formed above the inner cylinder, and four eddies exist symmetrically about the vertical centre line. It seems that a critical aspect ratio rr may exist to distinguish whether one plume or three plumes exist in the isotherms, and whether two eddies or four eddies exist in the streamlines. This may lead to further numerical and experimental investigations.

CONCLUSIONS

The global method of differential quadrature (DQ) is applied in this work to simulate the natural convection in a concentric annulus between a cold outer square cylinder and a hot inner circular cylinder. The vorticity-stream function formulation is solved by the DQ method in the curvilinear coordinate system. The super elliptic function is introduced to approximate the outer square boundary so that the coordinate transformation is set up by an analytical expression, and all the geometrical parameters are computed exactly. Numerical results for Rayleigh numbers range from 10^4 to 10^6 and aspect ratios between 1.67 and 5.0 are presented, which agree well with available data in the literature. It is found in this study that both the aspect ratio and the Rayleigh number are critical to the patterns of flow and thermal fields. It is suggested that a critical aspect ratio may exist at high Rayleigh number to distinguish the flow and thermal patterns.

It should be indicated that the coordinate transformation method used in this paper is general. It is applicable for different physical domains including the eccentric case. For the eccentric case, one just needs to change the transformation Equation (25).

REFERENCES

1. Kuehn TH, Goldstein RJ. An experimental and theoretical study of natural convection in the annulus between horizontal concentric cylinders. *Journal of Fluid Mechanics* 1976; **74**:695–719.
2. Warrington RO, Powe RE. The transfer of heat by natural convection between bodies and their enclosures. *International Journal of Heat & Mass Transfer* 1985; **28**(2):319–330.
3. Ekundayo CO, Probert SD, Newborough M. Heat transfer from a horizontal cylinder in a rectangular enclosure. *Applied Energy* 1998; **61**:57–78.
4. Stella F, Guj G. Vorticity–velocity formulation in the computation of flows in multi-connected domains. *International Journal of Numerical Methods in Fluids* 1989; **9**:1285–1298
5. Ghaddar NK. Natural convection heat transfer between a uniformly heated cylindrical element and its rectangular enclosure. *International Journal of Heat & Mass Transfer* 1992; **35**(20):2327–2334.
6. Deschamps V, Desrayaud G. Modeling a horizontal heat-flux cylinder as a line source. *Journal of Thermophysics and Heat Transfer* 1994; **8**(1):84–91.
7. Moukalled F, Acharya S. Natural convection in the annulus between concentric horizontal circular and square cylinders. *Journal of Thermophysics and Heat Transfer* 1996; **10**(3):524–531.

8. Liu Y, Phan-Thien N, Kemp R. Coupled conduction–convection problem for a cylinder in an enclosure. *Computational Mechanics* 1996; **18**:429–443.
9. Bellman RE, Kashef BG, Casti J. Differential quadrature: a technique for the rapid solution of nonlinear partial differential equations. *Journal of Computational Physics* 1972; **10**:40–52.
10. Shu C, Richards BE. Application of generalized differential quadrature to solve two-dimension incompressible Navier–Stokes equations. *International Journal of Numerical Methods in Fluids* 1992; **15**:791–798.
11. Shu C, Richards BE. Parallel simulation of incompressible viscous flows by generalized differential quadrature. *Computations and Systems Engineering* 1992; **3**:271–281.
12. Shu C, Chew YT, Khoo BC, Yeo KS. Application of GDQ scheme to simulate incompressible viscous flows around complex geometries. *Mechanical Research Communication* 1995; **22**:319–325.
13. Shu C, Chew YT, Khoo BC, Yeo KS. Solutions of three-dimensional boundary layer equations by global methods of generalized differential-integral quadrature. *International Journal of Numerical Method Heat Flow F* 1996; **6**(2):61–75.
14. Shu C, Chew YT. Fourier expansion-based differential quadrature and its application to Helmholtz eigenvalue problems. *Communications in Numerical Methods in Engineering* 1997; **13**:643–653.
15. Shu C, Xue H. Explicit computation of weighting coefficients in the harmonic differential quadrature. *Journal of Sound and Vibration* 1997; **204**:549–555.
16. Bert CW, Malik M. Differential quadrature method in computational mechanics. *Applied Mechanical Review* 1996; **49**(1):1–28.
17. Bellman RE, Casti J. Differential quadrature and long-term integration. *Journal of Mathematical Analysis & Applications* 1971; **34**:235–238.
18. Shu C. *Differential Quadrature and its Application in Engineering*. Springer-Verlag, London, 2000.
19. De Vahl Davis G. Natural convection of air in a square cavity: a bench mark numerical solution. *International Journal of Numerical Methods in Fluids* 1983; **3**:249–264.